Combined Langmuir probe, electrical and hybrid modelling characterization of helium glow discharges

G Bánó[1,3]**, P Hartmann**[1]**, K Kutasi**[1]**, P Horváth**[1]**, R Plašil**[2]**,
P Hlavenka**[2]**, J Glosík**[2] **and Z Donkó**[1]

[1] Research Institute for Solid State Physics and Optics of the Hungarian Academy of
Sciences, POB 49, H-1525 Budapest, Hungary
[2] Mathematics and Physics Faculty, Department of Electronics and Vacuum Physics,
Charles University Prague, V Holešovičkách 2, Prague 8, Czech Republic

E-mail: bano@sunserv.kfki.hu

Abstract
We present a systematic study of electrical characteristics and Langmuir
probe measurements on plane-parallel electrode helium glow discharges
operated in normal and abnormal glow regimes. The experimental studies
are complemented with numerical modelling based on a hybrid approach
combining fluid and particle descriptions of the discharge plasma.
A comparison between the experimental data and the two-dimensional
modelling results is presented. The temperature of slow Maxwellian
electrons is found to be $\approx$0.055 eV in the negative-glow region nearly
independent of the discharge conditions. This temperature value is used as
an input parameter of the hybrid model. Good agreement is obtained
between the calculated spatial density distribution of electron impact
excitation events and the CCD image of the light emission from the
discharge. The calculated electron densities are 1.3–2 times higher than
the corresponding Langmuir probe data; the possible reason for these
differences is discussed.

1. Introduction

Noble gases, helium among them, have been used as buffer
gases in a variety of plasma sources. In contrast to
the wide usage of this gas, relatively few reliable data
are available for electrical characteristics, charged particle
densities and electron temperature in the cathode region of
simple parallel plate electrode (PPE) low-pressure helium
discharges. The breakdown behaviour and the properties of
low-current (Townsend) discharges in the PPE arrangement
have been investigated in [1]. Excitation in low-current PPE
discharges and breakdown in helium at low pressures and very
high electric field to gas density ratios have been studied in [2].
Studies of the role of molecular ions in PPE He glow discharges
up to pressures of 60 mbar have been reported in [3, 4]. The

temperature and density of cold negative-glow electrons have
been determined by Lawler and co-workers in [5, 6].

In this paper we focus on the cathode region of a low-
pressure helium glow discharge, which consists of the cathode
sheath and the negative glow. A better understanding of
such plasmas is necessary for the optimization of glow-
discharge applications. To achieve this goal it is important to
develop discharge models capable of describing the physical
properties of the investigated plasmas. On the other hand,
the results and consistency of the models can only be
tested if reliable experimental data are available. Simple
discharge geometries, such as the plane-parallel electrode
glow discharge, can favourably be used to test the models.
Accordingly, we carried out Langmuir probe measurements in
the negative-glow region of a plane-parallel electrode helium
glow discharge complemented with a thorough determination
of voltage–current characteristics.

---

[3] Author to whom any correspondence should be addressed.

From the modelling point of view, the simulation technique applied has to take account of the non-local character of the cathode region: the significant gradient of the electric field in the cathode sheath results in a non-hydrodynamic transport of charged species. Moreover, there is a non-Maxwellian electron energy distribution in the discharge. The most important criterion for the models is to reproduce the relevant plasma parameters; however, the robustness and flexibility of the computation method is also important. In the optimal case the model can easily be applied for more sophisticated discharge arrangements calculating their properties without the need for simplifying assumptions.

The two-component fluid description of charged particles (usually positive ions and electrons) represents the simplest self-consistent approach for the description of glow-discharge plasmas. In fluid models charged particles are characterized by their density and temperature values, and the non-Maxwellian character of the electron distribution function (EDF) is not taken into account. The continuity and momentum transfer equations of charged particles are solved together with the Poisson equation to give a description of the charged particle density and the electric potential distribution. The rate of ionization events (which is the source of charged particles) is calculated locally on the basis of the electric field. It was shown in [7] that the fluid approach fails to reproduce the most important plasma parameters. For example, the density of charged particles in the negative glow may be underestimated by orders of magnitude.

A significant improvement in the fluid model is obtained using a hybrid scheme [8–12], where a kinetic approach is applied to simulate the motion of fast particles (which are responsible for the ionization of the buffer gas) while fluid description is preserved to follow the transport of slow electrons and ions [13]. The non-local transport of fast particles in the cathode region is usually described by Monte Carlo (MC) simulation. The ionization source functions obtained from the MC calculation serve as an input for the fluid code. It is noted that a 1D hybrid combination of the fluid code with the solution of the electron Boltzmann equation (which is an alternative approach that may replace the time-consuming MC simulations) was reported for the case of a hollow-cathode discharge [14]. In general the fluid-MC hybrid approach results in a convincing and flexible description of the whole cathode region. Both the cathode sheath and the negative glow are calculated within the framework of the same formalism, which allows for convenient handling of 2D problems. A weakness of the hybrid approach is connected to the fluid part of the model, where the transport of charged particles is treated locally and the EDF of slow electrons (having energies below the first excitation potential) is taken to be Maxwellian. A fixed electron temperature is usually assigned to these 'bulk' electrons, which may lead to significant errors [7]. Additional experimental data are expected to enhance the reliability of modelling calculations. In [15], for high current conditions the slow electron temperature has been fitted to reproduce the measured discharge voltage values. An average electron temperature calculated on the basis of an energy-balance equation has been used in the fluid code applied in the modelling studies of [16]. The temperature of slow electrons can also be determined experimentally as is done in the present work.

In principle the imperfection of hybrid models can be overcome by a fully kinetic description of the investigated plasmas. One possibility is to use the particle-in-cell modelling scheme complemented with the MC description of collision processes (PIC/MCC). However, up to now the PIC/MCC code was found to have serious inconsistencies in the case of dc discharges [7,17]. An analytical model treating different groups of electrons in a kinetic way was published in [18]. The electrons are divided into three groups here: slow Maxwellian electrons characterized with a temperature T_e, slow intermediate (superthermal) electrons representing a hot tail of the EDF and fast electrons having energies above the first excitation potential of the buffer gas. Such a description of the EDF is more realistic as compared to the one applied in the fluid-MC hybrid models. The energy balance of slow Maxwellian (trapped) electrons in a negative-glow plasma was studied in detail in [19, 20] using a similar analytical description as in [18]. The temperature of slow Maxwellian electrons was calculated based on the electron Boltzmann equation and an energy-balance equation. It is noted that all the mentioned analytical models rely on some crude simplifications introducing sharp boundaries between different space and energy regions thereby limiting their flexibility for describing various discharge arrangements. A recent review on the state-of-the-art for the simulation of electron kinetics in gas discharges based on the numerical solution of the Boltzmann equation was given in [21]. A MC model (comprising electron–electron collisions) capable of calculating the whole EDF was reported in [22]. Another possibility of self-consistent kinetic modelling of an entire dc discharge was demonstrated by Parker et al in [23] using the 'convective scheme' to model the cathode fall and the negative-glow regions without breaking the electron energy distribution function in components. It would be desirable to carry out a detailed comparison of all the above models in the future.

Let us assume that the ambipolar electric field obtained from the fluid description of the quasi-neutral negative-glow region is realistic, which means that the ambipolar field is mostly driven by slow Maxwellian electrons characterized by their temperature. The same approximation was made in the analytical models in [19, 20]. It follows that once the temperature of slow electrons is determined (e.g. experimentally) the overall flux of ions in the negative-glow region (where their transport is hydrodynamic) is described correctly by the fluid code. Of course, the fluid description of the electrons remains incorrect, but the diffusion loss of charged particles will be estimated in a realistic way. Consequently, the fluid-MC hybrid code may result in the correct density of charged particles in the negative glow provided that the size of the negative glow and the source of electrons obtained from the MC routine are correct.

The aim of this paper is (i) to present experimental voltage–current characteristics of He normal/abnormal glows in a wide range of the pd (pressure $\times$ electrode separation) product, (ii) to determine charged particle densities and electron temperature for different operating conditions and (iii) to compare the experimental data with the results of a two-dimensional fluid-MC hybrid model. Section 2 describes the experimental arrangement. The modelling approach is outlined in section 3. The experimental and modelling results

are presented and are compared with each other in section 4. Section 5 presents the conclusions of the paper.

2. Experimental

2.1. The dc helium discharge

The discharge tube consists of two PPEs situated inside a pyrex cylinder which prevents long-path breakdown (see figure 1). The electrodes are made of copper with a diameter ($2R$) of 7.7 cm. The electrode separation (d) can be continuously varied between 1 and 3 cm.

The electrode construction is mounted inside a vacuum chamber which is pumped down to a base pressure of the order of 10^{-7} mbar. The operating pressure (p) is established by using 5–10 sccm flow of pure (6.0) helium. The gas is further purified by passing through a liquid nitrogen trap prior to entering the vacuum chamber. Before the measurements the surface of the cathode is treated by a medium current discharge in helium (≈ 4 mA) for ≈ 15 min.

The voltage–current characteristic of the discharge is scanned using a computer controllable direct current power supply (type Stanford Research Systems, PS 325) connected to the discharge through a serial resistor $R_s = 66$ kΩ. The current range of 1–10 mA is scanned by applying first a positive and then a negative voltage ramp (in ≈ 50 steps with a step time of ≈ 2 s), fast enough to avoid excessive heating of the cathode [24]. By applying dc excitation the heating of the filling gas may, on the other hand, be significant, but this effect is reduced by the gas flow, and it can be accounted for in the models.

The spatial distribution of the light emitted from the discharge is detected through a 10 cm diameter side-window of the discharge chamber by means of a CCD camera. The camera—sensitive in the visible spectral region—is equipped with a $f = 200$ mm lens and is placed ≈ 2 m apart from the discharge.
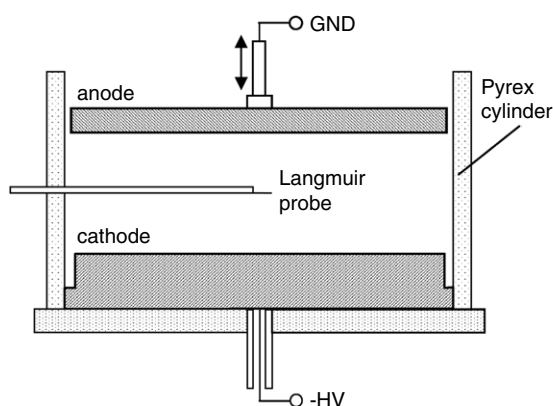

Figure 1. Schematic view of the discharge tube. The whole construction is placed inside a vacuum chamber. The vertical position of the anode electrode is adjusted by means of a manual vacuum feed-through translator. There are four ≈ 1 mm wide, ≈ 20 mm long vertical slits cut into the pyrex cylinder (not shown) to facilitate the gas flow through the discharge region. The probe measurements are carried out for an electrode separation of $d = 3$ cm with the probe being positioned approximately at the tube axis, 1.5 cm above the cathode. The probe support as well as the probe itself are mounted in a horizontal direction.

2.2. Langmuir probe measurements

The temperature and the density of slow electrons are determined experimentally for the $d = 3$ cm discharge by means of a cylindrical Langmuir probe, which is positioned at the discharge centre. The obtained electron temperature is used as an input parameter in the computer simulation of the discharge (see section 3); the measured density data are compared with the modelling results in section 4.

In order to minimize the disturbance of the plasma it is important to keep the dimensions of both the probe and the probe support small [25]. The probe is 2.5 mm long and is made of a 20 μm diameter tungsten wire. The applied support consists of two coaxial glass tubes with the diameter of the outer one being 0.5 mm (see figure 2). Preliminary test measurements were carried out in the same discharge tube using a 2 mm diameter probe support with a 40 μm diameter, 2.5 mm long probe. In this case—due to the significant depletion of charged particles by the probe and its support—the obtained electron density was more than 10 times smaller as compared with the one measured with the recent probe. This fact indeed stresses the importance of the small probe size. It is noted that one can still expect a certain level of plasma density reduction in the vicinity of our recent probe.

In the experimental arrangement significant deposition of sputtered metal atoms takes place on the discharge tube walls. After a few hours of discharge operation a thin copper layer (visible to the eye) also builds up on the probe support. It is necessary to avoid the formation of an electrical contact between the probe surface and the metal layer deposited on the support. For this reason the inner glass tube of the probe support is made 1 mm shorter as compared with the outer one. This way we can keep the active probe surface area constant for an extended time period.

On the other hand, the metal atoms deposited onto the probe surface may distort the measurement. To prevent the probe surface from being covered by a sputtered metal layer the probe is regularly cleaned by ion bombardment. The following steps are applied to keep the probe surface clean during the measurements. Before the acquisition of each point on the voltage–current probe characteristic curve the probe is connected to a negative bias voltage of -120 V by means of a relay (through a 100 kΩ resistor). Ions bombarding the probe during the 100 ms cleaning period are capable of removing the deposited copper atoms (and other impurities) from the surface; a clean tungsten surface is observed after dismounting the probe setup. At the end of the cleaning period the probe is connected to the prescribed voltage. After a time lag of 25 ms the current and voltage values are recorded for 100 ms by a PC lab card with a sampling frequency of 10 kHz. For each point on the probe characteristic curve the
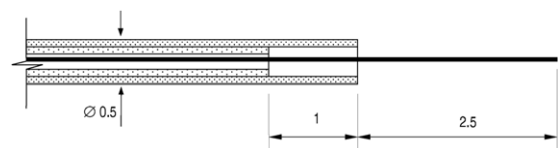

Figure 2. Scheme of the Langmuir probe showing the major probe dimensions in mm units. The probe support consists of two coaxial glass tubes; the probe is made of a 20 μm diameter tungsten wire.

average of the obtained 1000 values is calculated. This way the effect of a possible 50 Hz noise is significantly suppressed. One has to keep in mind that due to the different materials of the grounded anode (copper) and the probe (tungsten) there is always a contact potential between the probe and the anode which is not detected by the measurement system. This contact potential may change significantly with changing surface conditions (cleanliness, temperature, etc) resulting in a voltage shift of the probe characteristics relative to the voltage that is applied and detected externally. Due to this fact the precision of the plasma potential values obtained from the probe measurements is always limited by the uncertainty of the contact potential. Moreover, surface conditions may be non-uniform for contaminated probes giving different contact potentials for different surface areas. Without the above-mentioned excessive cleaning we observed the typical behaviour of contaminated probes giving an overestimated electron temperature, see e.g. [26].

It is noted that due to the cleaning procedure a single probe characteristic takes about 1–2 min to record. Due to this fact we cannot avoid heating up the cathode during the probe measurements. Thus, in contrast to the voltage–current characteristic measurements (described in the previous section) the Langmuir probe data belong to a near equilibrium cathode temperature. The elevated temperature results in a higher discharge voltage, which is specific for the present apparatus. In the following we only present experimental probe data obtained at conditions, where the difference in discharge voltage values obtained in the measurements of the electrical characteristics and during Langmuir probe measurements does not exceed 30 V.

3. Numerical model

Our numerical simulations are based on the fluid-MC hybrid modelling approach. The fast electrons with energies above the lowest excitation potential are followed by a MC routine; the slow electrons, which are no longer able to excite the gas, as well as the positive ions are described by a fluid model.

The fundamental quantities in the fluid model are the electric potential and the densities of slow electrons and He$^+$ ions. The particle balance for these species is expressed by the continuity equations:

$$\frac{\partial n_e}{\partial t} + \nabla \vec{\phi}_e = S_e \qquad \text{and} \qquad \frac{\partial n_i}{\partial t} + \nabla \vec{\phi}_i = S_i, \quad (1)$$

where n_e and n_i are the electron and the ion densities, $\vec{\phi}_e$ and $\vec{\phi}_i$ are the electron and the ion fluxes, while S_e and S_i are the source functions of slow electrons and He$^+$ ions. The fluxes are calculated on the basis of the drift–diffusion approximation:

$$\vec{\phi}_e = -\mu_e n_e \vec{E} - \nabla(n_e D_e) \quad \text{and} \quad \vec{\phi}_i = \mu_i n_i \vec{E} - \nabla(n_i D_i),$$
$$(2)$$

where μ_e and μ_i are the mobilities of electrons and ions, respectively. $\vec{E} = -\nabla V$ is the electric field and V is the potential:

$$\nabla^2 V = -\frac{e}{\varepsilon_0}(n_i - n_e), \quad (3)$$

where e is the elementary charge and ε_0 is the permittivity of free space. The diffusion coefficients D_e and D_i are

calculated from the Einstein relation: $D = \mu k_B T$, where k_B is the Boltzmann constant and $k_B T$ is the characteristic energy for the given species. In our calculations we take $k_B T_e$ as derived from our probe measurements (see section 4.2) and $k_B T_i = 0.026$ eV. The mobility of electrons is given by $\mu_e p = 133$ cm^2 V^{-1} s^{-1} mbar, and the He$^+$ ion mobility, μ_i, as a function of E/n is taken from [27]. It is noted that the validity limits of the chosen set of fluid equations as well as the suitability of the applied transport coefficients should be justified by detailed benchmarking as was proposed and discussed in [28]. Such a study is beyond the scope of this paper.

The fluid code is two-dimensional, while the MC routine is three-dimensional in space and in velocity space. The fluid equations together with the Poisson equation are solved on a uniform grid containing 80 (axial) $\times$ 30 (radial) points. The boundary conditions at the walls are zero density of particles and prescribed values of the electrode potentials (zero at the cathode and V at the anode). The electric potential distribution at the dielectric walls is calculated by adjusting $V(x, r = R)$ to achieve a flux balance of incoming and leaving charges at every wall segment (nearest gridpoint). The effective secondary electron emission yield (γ_{Cu}) of the copper cathode has a fixed value of 0.16 for all investigated cases, which is a good approximation based on the data of [29], while the electron yield for the walls γ_{pyrex} is fixed at 0.2. The fluid equations are solved using an implicit integration scheme [8] with a typical integration time step of the order of 10 ns.

The electrons are traced by MC simulation from the moment of their emission from the cathode or their creation in an ionization process until (i) their total (kinetic + potential energy) falls below the first excitation energy of the gas or (ii) they reach the anode. For the primary electrons backscattered to the cathode we take into account elastic and inelastic reflection/re-emission [30] and absorption at the cathode. Energetic electrons hitting the anode can be absorbed or reflected and can initiate secondary electron emission [29].

The trajectory of a particle between successive collisions is followed by direct integration of the equation of motion:

$$m\frac{d^2 \vec{r}}{dt^2} = e\vec{E}(\vec{r}), \quad (4)$$

where m and e are the mass and the charge of the particle, respectively. The free path is assigned statistically and the positions of the collisions are calculated from

$$\int_{s_0}^{s_1} n\sigma[\varepsilon(s)]\, ds = -\ln(1 - R_{01}), \quad (5)$$

where s_0 is the position of the last collision and s_1 is the position of the next collision measured on the curvilinear abscissa s; n is the background gas density, σ is the sum of cross sections of all possible elementary processes, ε is the kinetic energy of the particle and R_{01} is a random number with uniform distribution in the [0, 1) interval [31].

The types of collisions which occur after the free flights are chosen statistically, taking into account the values of cross sections of different processes at the energy of the colliding particle. In the gas phase we take into account elastic, excitation and ionization collision processes of electrons with

the background He gas [32]. The initial energy of the electrons leaving the cathode is chosen randomly between 0 and 10 eV [33], and their initial velocity is set perpendicular to the cathode surface. The scattering of the electrons in ionization and excitation collisions is assumed to be isotropic.

The fluid and MC routines are run iteratively. A serial resistor applied in the experiments is also taken into account in the modelling scheme. The external voltage applied to the resistor and the discharge is adjusted during consecutive computation steps until the converged discharge current matches the experimental value.

4. Results and discussion

4.1. Discharge voltage

In this section we present the experimentally determined voltage–current characteristics. Figures 3(*a*)–(*f*) display the discharge voltage as a function of I/p^2 for six different pd values, as follows: 9, 7.5, 6, 4.5, 3 and 2.5 mbar cm. Each figure shows measurements performed for four different electrode separations: 1, 1.5, 2 and 3 cm. The voltage is presented as a function of the reduced current I/p^2 instead of the reduced current density j/p^2, since the current density on the cathode may be radially inhomogeneous [34, 35]. It is noted, however, that in abnormal glow discharges spatial uniformity of the current density is expected to be much better than even in the Townsend regime.

At higher pd values, see figures 3(*a*)–(*d*), we can observe an almost perfect scaling of the voltage with I/p^2 for the different values of d (the four measured curves nearly overlap). This scaling brakes at $pd = 3$ mbar cm, figure 3(*e*), where the discharge of 3 cm electrode separation needs a higher operation voltage. This clearly indicates the appearance of additional losses of charges in the system, i.e. the effect of the tube wall. In fact, the effect of the walls on the discharge characteristics at a given pd value depends on the ratio of the electrode separation to the electrode diameter d/D. In our system the importance of the charge losses on the walls can be observed at the $d/D \geqslant 0.4$ and the $pd \leqslant 3$ mbar cm conditions. Figures 3(*e*)–(*f*) show that with decreasing pd at a given electrode separation (increasing of the electron mean free path) the effect of the walls on the characteristics increases.

At low currents the flat part of the characteristics indicates that the discharge is operating in the normal regime. In the high pd cases the normal cathode fall voltage is $U_n \approx 151$ V (about 15% smaller than the $U_n = 177$ V published in [36]), see figure 3(*a*). Figures 3(*a*)–(*d*) show that U_n increases with decreasing pd and reaches the value of 230 V at $pd = 2.5$ mbar cm. The reduced normal current density j_n/p^2 is found to be $\approx 2\,\mu\text{A cm}^{-2}\,\text{mbar}^{-2}$.

4.2. Evaluation of probe characteristics

A typical probe characteristic obtained at 2.25 mbar helium pressure and discharge current of 2 mA is shown in figure 4, where the absolute value of the probe current $|I_p|$ is plotted on a logarithmic scale as a function of the applied voltage. Comparative studies of Langmuir probe evaluation techniques in non-Maxwellian plasmas have been reported in [37]. During the evaluation, we calculate the second derivative of the total
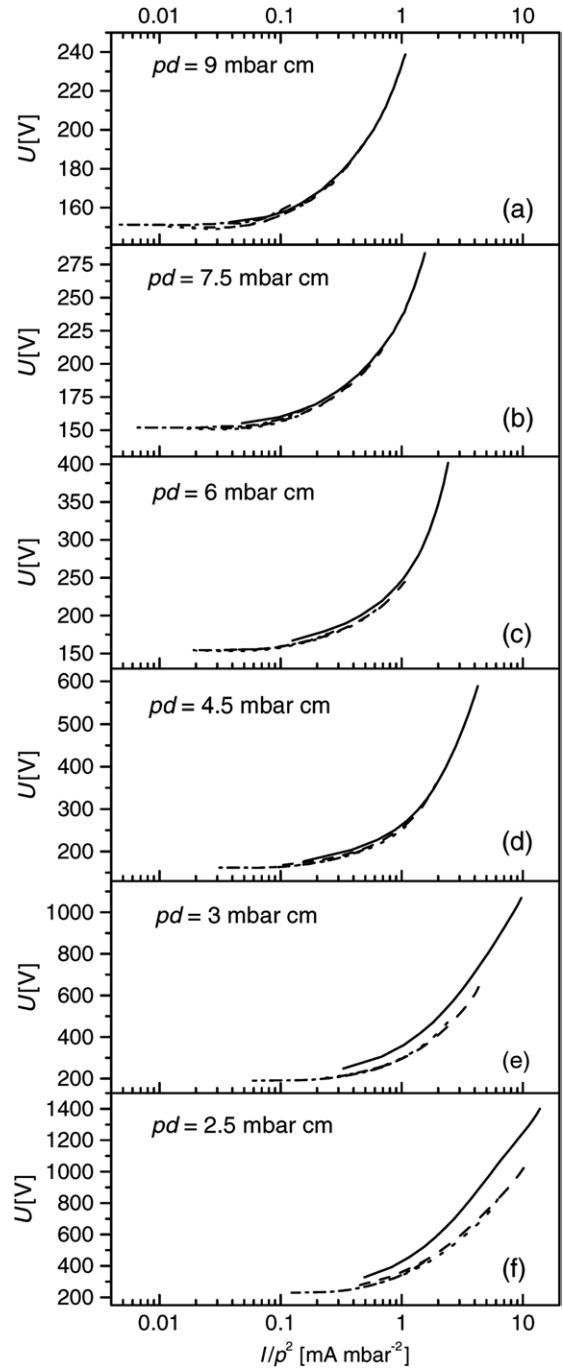

Figure 3. Measured discharge voltage as a function of I/p^2 for different pd values. $I/p^2 = 1$ mA mbar^{-2} corresponds to $j/p^2 = 0.0215$ mA cm^{-2} mbar^{-2} when a homogeneous current density distribution is assumed. The different lines in the figures belong to different electrode separations as follows: —— 3 cm, – – – 2 cm, - - - - 1.5 cm, — · — 1 cm.

probe current first (not shown in the figure). The position of the effective plasma potential U_{pl}^{eff} (which is the plasma potential shifted by the contact potential) is chosen to be at the zero crossing of the second derivative curve. A preliminary estimate of the electron temperature is obtained by fitting the second derivative with an exponential decay in the electron retardation region close to the plasma potential. Next, the ion part I_i of the probe current is estimated. There are numerous theories
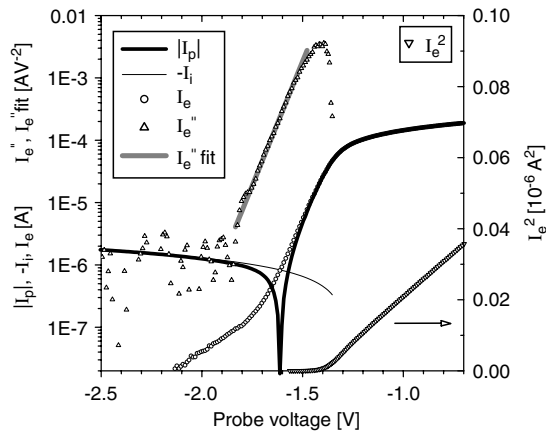
Figure 4. A typical Langmuir probe characteristic obtained at 2.25 mbar helium pressure and discharge current of 2 mA. The absolute value of the probe current $|I_p|$ is plotted as a function of the applied voltage. Other curves: left axis: $-I_i$—fit to the ion current extrapolated to the effective plasma potential (at -1.35 V), I_e—the electron current, I_e''—second derivative of the electron current, I_e'' fit—an exponential fit to I_e'' providing the temperature of slow electrons (T_e is 0.057 eV here); right axis: I_e^2—the square of the electron current, which is fitted by a linear dependence to obtain the density of slow electrons ($n_e = 3.1 \times 10^{16}$ m^{-3}).

describing the collected ion current under different plasma conditions (see e.g. [38] and the references cited therein). For the sake of simplicity and because the further evaluation does not rely much on the ion current, here the ion current is fitted (in the far negative voltage region) by the empirical formula given in [39]: $I_i = I_0(1 + (U - U_{pl}^{eff})/kT_e)^\kappa$. This dependence is then extrapolated to the effective plasma potential, as shown in figure 4. Once the ion current is obtained the electron current I_e is calculated as $I_e = I_p - I_i$. The near exponential decay of the electron current in the retardation voltage region indicates the presence of numerous slow electrons in the plasma. Another group of more energetic electrons is responsible for the excessive electron current driven to the probe at even lower voltages. The second derivative of I_e (see figure 4) is calculated and fitted by an exponential to obtain the temperature of slow electrons.

The electron density n_e is evaluated from the electron saturation region of the probe characteristic based on orbital motion limited (OML) theory. According to this model the square of I_e (depicted in figure 4) depends linearly on the voltage, whose relation indeed shows up in the present measurement. The density of slow electrons can be determined from the slope of I_e^2. Under all the discharge conditions investigated in this paper the Debye shielding length λ_D remains in the range of $2r_p > \lambda_D > 0.5r_p$, where r_p is the probe radius. It follows that the smallest λ_D values (which belong to higher discharge currents) are below the limit of $\lambda_D \approx r_p$ for which OML theory still applies (see [37] and the references cited therein). To verify the results of OML theory the electron density is also calculated using the Druyvesteyn procedure [37]. It is found that the densities obtained from the two independent evaluation procedures agree within 30% for all the discharge conditions covered here and do not show any correlation with the λ_D values.

The temperature of slow electrons as evaluated from the exponential decay of the I_e'' curve (see figure 4) is depicted
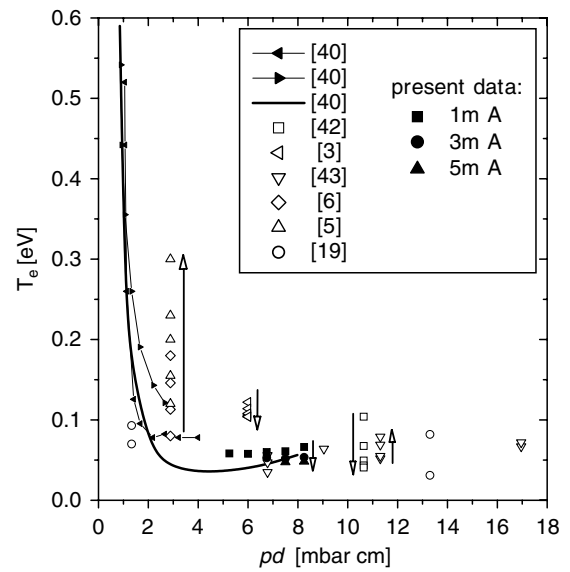

Figure 5. The temperature of slow electrons in the helium negative-glow dc discharge region as a function of pd, where p is the pressure and d is the characteristic size of the discharge. The present Langmuir probe data (taken at $d = 3$ cm) are shown together with the results of earlier measurements and theoretical predictions available in the literature. The arrows are pointing towards the increasing current values.

for different discharge conditions in figure 5. The new experimental results are shown together with other values measured or calculated for dc negative-glow helium plasmas that are available in the literature.

The electron temperature data are presented as a function of pd, which is the scaling factor proposed by Franck *et al* [40, 41] for the case when ambipolar diffusion represents the major loss mechanism for slow electrons. It is important to keep in mind that the geometry of the discharges studied by different authors and the method of obtaining the electron temperature data are not the same. The distance d used to create figure 5 is taken as the smallest characteristic size of the discharge tube surrounding the studied negative-glow region. Due to very different discharge conditions one would not expect a perfect pd scaling for all the presented data. The average value of the present data, $T_e = 0.055$ eV (showing negligible pressure dependence), fits the general behaviour of other points very well. It can be seen that except for low pd values most of the available data indicate electron temperatures below 0.15 eV.

Regarding the current dependence of the electron temperature at a given pressure we find no general agreement between the experimental results collected in figure 5. No current dependence was found by Franck *et al* [40, 41] who determined the electron temperature from both the reversal of a radial ambipolar electric field in a longitudinal magnetic field and using a Langmuir probe. Three out of the six other measurements indicate an increasing T_e value with increasing discharge current, and the opposite is true for the remaining three data sets. The tendency in the current dependence is indicated in figure 5 by arrows pointing towards the increasing current values. Based on these data (taking into account the experimental uncertainties as listed below) it is difficult to

give a statement as to what should the current dependence look like. The probe measurements of Anderson [42], our present Langmuir probe measurements as well as previous optical emission spectroscopy measurements [3] show lower T_e towards higher current values. There is a possibility of some inherent errors while using Langmuir probes for electron temperature measurements. Such errors can partially be due to inefficient cleaning of the probe. For example, the cleaning procedure applied here is probably more effective at higher currents (higher ion densities). Anderson [42] presumed that weak dc fields from the probe penetrate into the plasma over a sufficient number of mean free paths of the diffusing electrons and raise their mean random energy. The heating effect of non-thermal electrons released by the metastables impinging on the probe surface has been discussed by Powers [43]. In the case of the optical emission method applied in [3] the requirement of local thermal equilibrium (LTE) for slow electrons and the upper levels of the $2p^3P$–nd ^3D He I transitions ($n \geqslant 6$) may not be completely fulfilled [44]. A pronounced increase in T_e with increasing discharge current was reported by Lawler and co-workers [5, 6] and also by Powers [43]. The purity of the experimental apparatus used in these measurements seems to be a few orders of magnitude better as compared with the cleanliness reached in the other papers. This would indicate a high reliability of these data sets; however, there are other circumstances and objections complicating the situation. The method of Lawler and co-workers is based on a combination of experimental (laser diagnostics) data and results of MC simulations—providing the density and the temperature of slow electrons in a fully coupled way. The complicated procedure did not yield a monotonously increasing electron density with increasing current values, which may be an indication of some inconsistencies in the applied assumptions. There is very good agreement between the spectrometric and the Langmuir probe results of Powers [43], giving increasing T_e with increasing current (only the spectrometric data are shown in figure 5). Unfortunately, Powers used brush cathodes and also the discharge arrangement applied in [43] allowed for a hollow-cathode effect taking place in the cathode region. It is known that the electron temperature may be different in hollow-cathode discharges as compared with the planar arrangement [19]. Finally, according to theoretical predictions of Arslanbekov and Kudryavtsev [19] given for a model negative-glow helium discharge region (confined in a 2 cm diameter tube and characterized by the pressure and a spatially uniform ionization rate), higher electron temperature belongs to higher charge densities. It is concluded here that further studies are required to clarify the experimental inconsistencies in the current dependence of the slow electron temperature.

4.3. Modelling results and comparison with experiments

The calculated discharge voltage values are shown in figure 6 together with the corresponding experimental data. The calculated voltage exceeds the measured one by 25–50 V depending on the discharge current. The slight pressure dependence of voltage curves is well reproduced by the calculation. The differences may primarily be attributed to the uncertainty of the applied secondary electron emission coefficient and the simplifications of the model itself. To
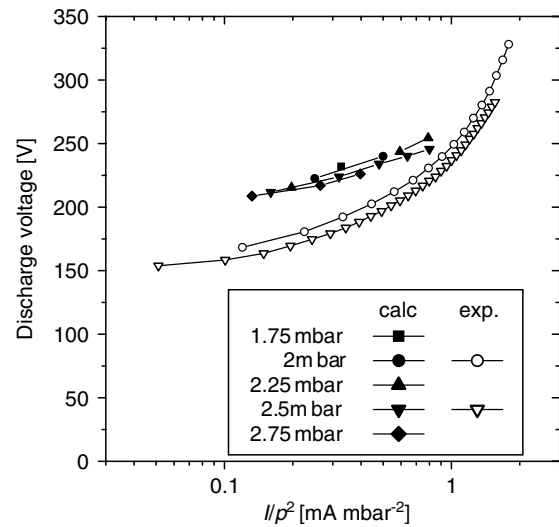
Figure 6. Calculated and experimental discharge voltage as a function of I/p^2 for $d = 3$ cm at different pressures.

improve the model the dependence of γ on the discharge conditions should be taken into account as was done for the case of argon discharges [7]. A detailed comparison of 1D and 2D hybrid models [45] has indicated that using constant γ a pronounced difference between 1D and 2D results shows up at lower pressure values (around 1 mbar for the 3 cm gap), where 2D modelling satisfactorily reproduces the measured experimental voltage curves. A detailed investigation of the calculated discharge voltage in a large pressure range is beyond the scope of this paper.

The spatial distribution of the light emission from the discharge detected by a CCD camera is shown in the upper left panel of figure 7. In optically thin plasmas the spatial distribution of the light emission strongly correlates with the different excitation processes. The contour plot showing the density of electron impact excitation events—as obtained from the model—is depicted in the upper right panel of figure 7. There is very good agreement between the experimental and the simulated distributions. The computer model can reproduce both the general shape of the CCD image and the position of the maximal light intensity.

The distribution of the calculated electric potential and the density of helium ions in the discharge tube is shown in the lower panels of figure 7. There is a strong electric field in the cathode dark space near the cathode. The potential value in the negative glow higher than the anode potential is a manifestation of the field-reversal effect (see, e.g. [46]). Because of the uncertainties of the plasma potential determination by the Langmuir probe (see the discussion in section 2.2) it is not possible to measure the extent of the field reversal in the recent experiment.

It is noted that there is a pronounced radial dependence of all the physical properties depicted in figure 7, which is a feature that can only be reproduced by two-dimensional discharge models.

The spatial dependence of the electric potential and the helium ion density at the tube axis—calculated for the $I = 1$ mA, $d = 3$ cm discharge—is shown for different pressures in figure 8. The position of the maximal ion density is
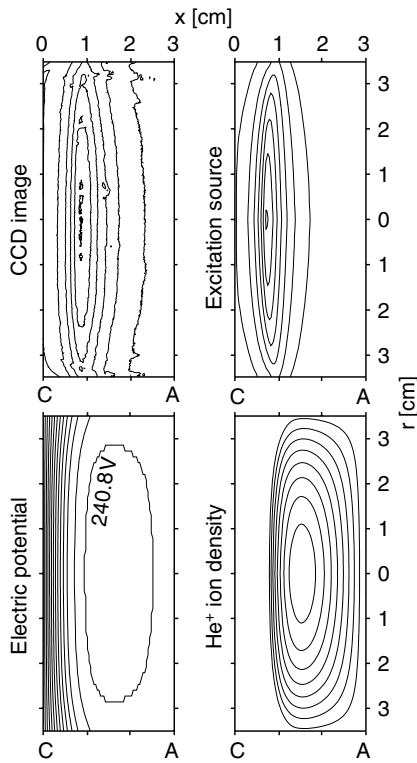
Figure 7. Upper left: A CCD image of the light emission from the discharge. Upper right: calculated spatial density distribution of electron impact excitation events. The (radially symmetrical) modelling data are line-of-sight integrated this way making the distribution directly comparable to the CCD recording. Lower left: electric potential in the discharge region; the separation of the contour lines corresponds to $\Delta U = 20$ V except for the indicated value of 240.8 V. Lower right: distribution of helium ion density; $\Delta n_i = 1 \times 10^{16} \, \text{m}^{-3}$, $n_i^{\max} = 8.8 \times 10^{16} \, \text{m}^{-3}$. All data belong to $p = 2$ mbar, $I = 2$ mA, $U_{\text{calc}} = 240.4$ V conditions.

located approximately halfway between the electrodes and moves towards the cathode as the pressure increases. The density of ions in the cathode sheath $((2–3) \times 10^{14} \, \text{m}^{-3})$ is approximately two orders of magnitude smaller as compared with the maximal ion density in the negative-glow region. The width of the cathode sheath decreases with increasing pressure. At the tube centre—where the Langmuir probe is positioned—the model predicts a decreasing ion density towards higher pressure values. Figure 9 shows the calculated and the measured density data at the tube centre obtained for different discharge conditions. It can be seen that the calculated data are a factor of 1.3–2 higher than the measured values. The pressure and current dependence of the electron density obtained from the model is in qualitative agreement with the experiments. As was discussed in section 2.2, the presence of the Langmuir probe and the probe support in the discharge unavoidably leads to a depletion of the electron and the ion densities in the vicinity of the probe. This experimental error is possibly the major reason for the differences in the modelling results and measured data.

5. Conclusions

Experimental voltage–current characteristics and Langmuir probe measurements of the electron density and temperature
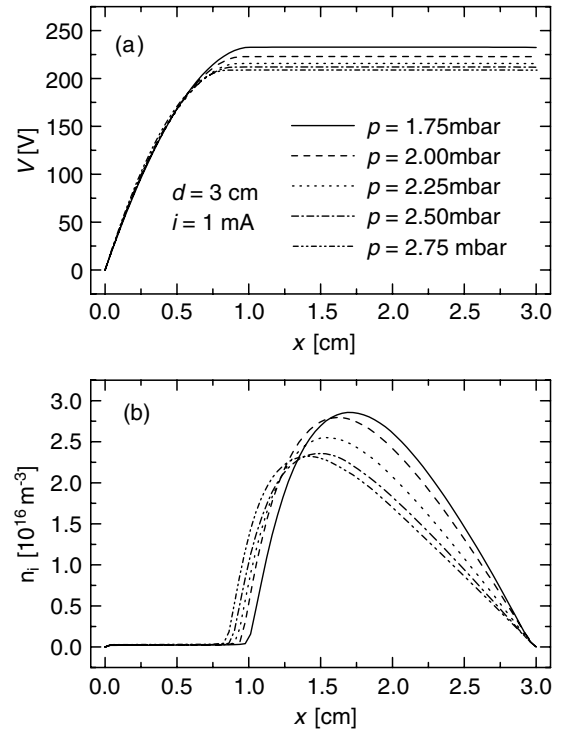

Figure 8. The calculated electric potential (*a*) and helium ion density (*b*) at the tube axis. The legend given in (*a*) applies for both panels.

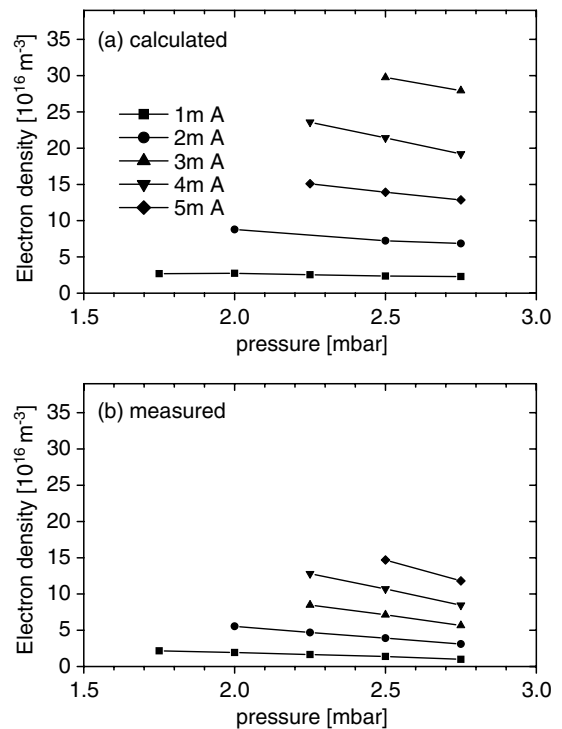**Figure 9.** Calculated and measured electron densities at different pressures and current values at the centre of the $d = 3$ cm discharge. The legend given in (a) applies for both panels.

have been presented for a helium glow discharge in a plane-parallel electrode arrangement. The temperature of slow Maxwellian electrons was found to be ~ 0.055 eV, nearly independent of discharge conditions (pressure and current).

This value has been used as an input parameter for a fluid-MC hybrid code, to avoid the need for assuming a value for T_e, as done usually in hybrid models. The calculated discharge voltage exceeds the measured values by 25–50 V depending on the discharge current. This difference is believed to originate mainly from the value of the secondary yield γ which we use. Assuming proportionality between the local rate of electron impact excitation events and the corresponding intensity of light emission from the discharge, the 2D hybrid model has been found to reproduce the spatial distribution of the light emission in the cylindrical PPE arrangement very well. An overall reasonable agreement has been found between measured and calculated electron density values in the negative glow. Higher density values have been predicted by the model as compared with the measurements; the general pressure and current dependence of the electron density has been reproduced by the calculations. The experimental density data are believed to be underestimated due to the fact that the charge density is depleted in the vicinity of the Langmuir probe and the probe support. Consequently, it is necessary to further improve the quality of the experimental electron density data to provide an input for testing the results of modelling calculations with higher precision.

It is concluded that hybrid modelling represents a powerful tool for modelling glow discharges and provides very good qualitative and reasonable quantitative description of the cathode region of glow discharges. Measurements of T_e in different discharge configurations may improve the accuracy of modelling calculations.

Acknowledgments

References

[1] Hartmann P, Donkó Z, Bánó G, Szalai L and Rózsa K 2000 *Plasma Sources Sci. Technol.* **9** 183
[2] Jelenković B M and Phelps A V 2005 *Phys. Rev.* E **71** 016410
[3] Kutasi K, Hartmann P and Donkó Z 2001 *J. Phys. D: Appl. Phys.* **34** 3368
[4] Kutasi K, Hartmann P, Donkó Z and Bánó G 2005 *Plasma Sources Sci. Technol.* **14** S1–8
[5] Den Hartog E A, Doughty D A and Lawler E A 1988 *Phys. Rev.* A **38** 2471
[6] Lawler J E, Den Hartog E A and Hitchon W N G 1991 *Phys. Rev.* A **43** 4427
[7] Donkó Z, Hartmann P and Kutasi K 2006 *Plasma Sources Sci. Technol.* **15** 178
[8] Boeuf J P and Pitchford L C 1991 *IEEE Trans. Plasma Sci.* **19** 286
[9] Bogaerts A, van Straaten M and Gijbels R 1995 *Spectrochim. Acta* B **50** 179
[10] Shidoji E, Ohtake H, Nakano N and Makabe T 1999 *Japan. J. Appl. Phys.* **38** 2131
[11] Donkó Z 2001 *Phys. Rev.* E **64** 026401
[12] Goedheer W J, Akdim M R and Chutov Yu I 2004 *Contrib. Plasma Phys.* **44** 395
[13] Fiala A, Pitchford L C and Boeuf J P 1994 *Phys. Rev.* E **49** 5607
[14] Sigeneger F and Winkler R 2005 *Plasma Chem. Plasma Process.* **25** 147
[15] Bánó G, Szalai L, Horváth P, Kutasi K, Donkó Z, Rózsa K and Adamowicz T M 2002 *J. Appl. Phys.* **92** 6372
[16] Brok W J M, Dijk J, Bowden M D, van der Mullen J J A M and Kroesen G M W 2003 *J. Phys. D: Appl. Phys.* **36** 1967
[17] Turner M M 2006 *Phys. Plasmas* **13** 033506
[18] Kolobov V I and Tsendin L D 1992 *Phys. Rev.* A **46** 7837
[19] Arslanbekov R R and Kudryavtsev A A 1998 *Phys. Rev.* E **58** 6539
[20] Arslanbekov R R and Kudryavtsev A A 1999 *Phys. Plasmas* **6** 1003
[21] Kolobov V I and Arslanbekov R R 2006 *IEEE Trans. Plasma Sci.* **34** 895
[22] Kushner M J and Vasenkov A V 2002 *Phys. Rev.* E **66** 066411
[23] Parker G J, Hitchon W N G and Lawler J E 1993 *Phys. Lett.* A **174** 308
[24] Bogaerts A and Gijbels R 2004 *J. Anal. At. Spectrom.* **19** 1206
[25] Godyak V A, Piejak R B and Alexandrovich B M 2004 *Plasma Sources Sci. Technol.* **11** 525
[26] Thomas T L and Battle E L 1970 *J. Appl. Phys.* **41** 3428
[27] Helm H and Elford M T 1978 *J. Phys. B: At. Mol. Phys.* **22** 3939
[28] Robson R E, White R D and Petrovic Z Lj 2005 *Rev. Modern Phys.* **77** 1303
[29] Hasselkamp D 1992 *Particle Induced Electron Emission II* (Berlin: Springer) p 43
[30] Thomas S and Pattison E B 1970 *J. Phys. D: Appl. Phys.* **3** 349
[31] Boeuf J P and Marode E 1982 *J. Phys. D: Appl. Phys.* **15** 2169
[32] Morgan W L, Boeuf J P and Pitchford L C 1998 *SIGLO Database, CPAT and Kinema Software* http://www.siglo-kinema.com/database
[33] Hagstrum H D 1953 *Phys. Rev.* **89** 252
[34] Donkó Z, Bánó G, Szalai L, Kutasi K, Rózsa K, Pinheiro M and Pinhao N 1999 *J. Phys. D: Appl. Phys.* **32** 2416
[35] Marić D, Kutasi K, Malović G, Donkó Z and Petrović Z Lj 2002 *Eur. Phys. J.* D **21** 73
[36] von Engel A 1965 *Ionized Gases*, (London: Clarendon) p 229
[37] Godyak V A, Piejak R B and Alexandrovich B M 1993 *J. Appl. Phys.* **73** 3657
[38] Sternovsky Z, Robertson S and Lampe M 2003 *J. Appl. Phys.* **94** 1374
[39] Nuhn B and Peter G 1977 *Proc. 13th Int. Conf. on Phenomena. Ionized Gases (Berlin)* p 97 (contributed papers)
[40] Franck G, Held R and Pfeil H D 1972 *Z. Naturf.* a **27** 1439
[41] Franck G, Held R and Pfeil H D 1972 *Z. Phys.* **256** 73
[42] Anderson J M 1960 *J. Appl. Phys.* **31** 511
[43] Powers R S Jr. 1966 *J. Appl. Phys.* **37** 3821
[44] Griem H R 1963 *Phys. Rev.* **131** 1170
[45] Hartmann P, Kutasi K and Donkó Z 2005 Comparison of one and two-dimensional hybrid modeling of low-pressure gas discharges *Proc. 27th ICPIG (Eindhoven, The Netherlands, 17–22 July 2005)* contribution 03-262
[46] Boeuf J P and Pitchford L C 1995 *J. Phys. D: Appl. Phys.* **28** 2083